EUROPEAN ORGANIZATION FOR NUCLEAR RESEARCH

EXCITATION OF MESONIC STATES IN $p\bar{p} \rightarrow ppX$ AT ISR ENERGIES

J.C.M. Armitage, P. Benz, G.J. Bobbink, F.C. Erné, P. Kooijman,
F.K. Loebinger, A.A. Macbeth, H.E. Montgomery, P.G. Murphy,
J.J.M. Poorthuis, A. Rudge, J.C. Sens, D. Stork, P. Strolin, J. Timmer

CERN, Geneva, Switzerland
Daresbury Laboratory, U.K.
Foundation for Fundamental Research on Matter, (F.O.M.), The Netherlands
University of Manchester, U.K.
University of Utrecht, The Netherlands
(CHM Collaboration)

Abstract

Data on the reaction $pp \rightarrow ppX$ are presented at two ISR energies, $s = 550$ and $935\ GeV^2$. The two measurements were made with a two arm spectrometer and a hodoscope detector. Evidence for resonance structure, in particular in the ρ and f region, will be discussed.

Submitted to the International Conference on High Energy Physics,
Tblisi, 15 - 21 July 1976.

May 1976

Introduction and apparatus

The study of mesonic clusters produced centrally in high energy pp collisions has so far proceeded mainly via correlation studies in high multiplicity events. A more quantitative approach is possible if the cluster mass is obtained from a missing mass measurement in pp → ppX. In the simplest case of the production of a low mass cluster as indicated in fig. 1, a study of the s, t, y and m dependence may reveal directly the exchanges involved. The diagram in fig. 1 assumes a configuration with two large rapidity gaps y_1 and y_2 with the exchange of reggeons with trajectories α_1 and α_2 respectively. A considerable range in s is necessary to establish the nature of these exchanges due to the logarithmic dependence of the rapidity gaps on s. The most favourable situation for studying the exchanges is realized if the central cluster is a resonance with known quantum numbers. In the limit of very high energies one might expect a dominating contribution from the exchange of two Pomerons.

The apparatus used for the present study consists of two forward spectrometers and 186 hodoscope counters at the CERN ISR. One of the spectrometers, placed downstream and on top of one ISR beam, has been described earlier[1]. It covers an angular range between 27 and 150 mrad in 10 mrad wide bins per setting and with an acceptance of 7.10^{-5} sr. It consists of 4 magnets with a total field integral of max 15 Tm, 3 gas Cerenkov counters, 21 spark chambers with magnetostrictive readout and trigger counters. Its momentum resolution is better than 0.8% FWHM. Proton identification is possible in the entire momentum range between 1 and 31 GeV/c. For the present investigation, however, no identification is necessary as the contamination with pions and kaons in the region of interest, $x > 0.7$, (x is the Feynman variable $x = 2p_L/\sqrt{s}$) is below 1%. A shorter version of this spectrometer consisting of the first magnet and 13 spark chambers has an acceptance of 3.10^{-4} sr, a magnetic field integral of max 6 Tm and a momentum resolution between 1 and 2% FWHM, depending on the momentum.

The second spectrometer is placed downstream and below the opposite ISR beam. It consists of one magnet with a max field integral of 2.8 Tm, 14 spark chambers and trigger counters. Its angular range is 12-95 mrad

and its acceptance about 7.10^{-5} sr. Its momentum resolution ranges between 1.4 and 3% FWHM depending on the momentum. The counter system consists of a barrel shaped central detector of 120 counters around the vacuum chamber bicone at the intersection[2] covering 2π in azimuth and 28^{o} to 152^{o} in polar scattering angle in the c.m. system, and 66 counters in the two forward directions.

The trigger for data taking consists of a coincidence between both spectrometers while additional particles in the hodoscope are recorded for off-line selection. In the measurements to be described the momentum acceptance of the first spectrometer covered a range in x between 0.7 and 1 and that of the second spectrometer between 0.5 and 1. To select events corresponding to the diagram in fig. 1 in the analysis, rapidity gaps can be imposed to some extent by requiring that no extra charged particles are emitted in the forward directions. The identification of known resonances with enhancements in the missing mass spectrum measured with the two spectrometers and the observation of their decay products at wide angle implies that no forward neutral particles are present in events with missing mass compatible with these resonances.

In the following, preliminary missing mass spectra will be presented, while the experiment is still taking data. A more complete analysis is in progress.

2. Experimental method

The missing mass m is defined by:

$$m^2 = (p_1 + p_2 - p_3 - p_4)^2 \qquad (1)$$

where p_1 , p_2 and p_3 , p_4 are the 4-vectors of the incoming and outgoing protons. For a precise measurement of the missing mass, the momenta and directions of the protons before and after the interaction have to be known with high accuracy. The momenta of the incoming protons can be determined to 0.2% from the determination of the ISR orbit of the colliding particle[3]. Their directions are known within

0.3 mrad from the betatron oscillation amplitude. The directions of the outgoing protons are experimentally determined to better than 1 mrad. A small contamination with events in which at least one of the outgoing protons scattered on magnet pole-pieces, scintillator counters or the ISR vacuum chamber, is removed in the analysis by requiring that the two reconstructed proton tracks meet in the intersection region within 1 cm.

The momentum scales of the two spectrometers with respect to the ISR momenta were calibrated with a precision of 0.1% using elastic events observed in both spectrometers separately with a single particle trigger. In the coincidence experiment elastic events are avoided by setting the spectrometers at unequal angles, and in the analysis stage by requiring at least a 10 mrad difference in production angle of the two forward protons. As equ. 1 can be approximated by:

$$m^2 = s\,(1 - x_1)\,(1 - x_2) - p_T^2 \qquad (2)$$

where p_T is the transverse momentum of the mesonic system, it is seen that the missing mass scale is known with a precision of $\sim 10^{-3}\ \sqrt{s}$, where $\sqrt{s}$ is ranging from 23 to 62 GeV in the present experiment. Values of the momentum resolution dx_1 and dx_2 at $x_1 = 1$, $x_2 = 1$ achieved up to now at various energies with the first spectrometer in its shorter version are indicated in table I.

TABLE I

Momentum accuracies in spectrometers 1 (short mode) and 2 (FWHM).

$\sqrt{s}$	dx_1	dx_2
23.5	0.013	0.014
30.5	0.010	0.014
44.7	0.015	0.017
52.9	0.015	0.028
61.6	0.02	0.030

Lines of equal mass are approximately hyperbolae in the x_1, x_2 plane, as indicated in fig. 2. The mass resolution derived from equ. 2, away from the point $x_1 = x_2 = 1$, becomes weakly dependent on the mass:

$$dm = \tfrac{1}{2}\sqrt{s}\left[dx_1^2 \exp(-2y_m) + dx_2^2 \exp(2y_m)\right]^{\frac{1}{2}} \qquad (3)$$

with y_m, the rapidity of the central cluster:

$$y_m = \tfrac{1}{2}\ln\left[(1-x_1)/(1-x_2)\right] \qquad (4)$$

Near to the point $x_1 = x_2 = 1$ one can assign a meaningful error only to m^2 (rather than m):

$$dm^2(x_1 \simeq x_2 \simeq 1) = s\, dx_1 dx_2 \qquad (5)$$

The mass resolution obtained from table I and eqn. 3 is shown as a function of y_m for various energies in fig. 3b. It depends strongly on s and y_m, with a minimum at $y_m=0$. To obtain an adequate sample with a good missing mass resolution, events with $|y_m| < 0.8$ are selected. As function of x_1 and x_2 this corresponds to a selection within the two straight lines of fig. 2. This procedure would lead to a loss of low mass events due to finite resolution effects. The straight line cut was therefore replaced by a hyperbolic cut as indicated in fig. 2. This approximately compensates for such a loss. At larger masses the hyperbolic cut becomes identical with a rapidity cut at $|y| < 0.8$. The mass dependence of the mass resolution for the selected sample of events is shown in fig. 3a; it is about 300 MeV (FWHM) for $\sqrt{s}$ = 23.5 and 30.5 GeV, and becomes progressively worse at higher energies. For the study of resonance production we therefore present data only for the two lowest energies.

Results and discussion

Fig. 4 shows a subselection of data at $\sqrt{s}$ = 23.5 GeV for charged particle multiplicity zero, $n_{ch}=0$ not counting the two forward

protons). It shows clearly the diffractive bands near the edge of phase space and an indication of a band in the f(1270) region going through the point $x_1 = x_2 = 0.945$. The extension of the diffractive band up to the point $x_1 = x_2 = 0.99$ can be attributed to the process $pp \rightarrow pp\pi^o$.

Missing mass spectra with as only selection the hyperbolic cut described above, are shown in fig. 5 for the two energies. A clear resonance signal stands out in the region of 1250 MeV at $\sqrt{s}$ = 23.5 and 30.5 GeV, and near 750 MeV in the 23.5 GeV data. A subsequent selection can be made on the directions of the decay particles. Fig. 6 shows a subselection with the requirement that no other charged particles than the protons are detected in the forward hodoscopes; this corresponds to a cut in the pseudorapidity η_c of the charged secondaries at $|\eta_c| \lesssim 1.6$. The resonance signals mentioned stand out more clearly, and the high mass region is increasingly suppressed. This suppression is connected with the multiplicity which increases with missing mass and reduces the probability that all decay particles of the central cluster(s) are confined to the rapidity region of ± 1.6 units covered by the central detector. A further selection on multiplicity in the central detector reveals peaks near the π^o mass and near m = 1250 MeV for $n_{ch} = 0$ in fig. 7, and the structures mentioned at 750 and 1250 MeV for $n_{ch} = 2$ in fig. 8. Two-body decay amongst the $n_{ch} = 2$ events can be identified by checking if the directions of the two charged decay particles are kinematically compatible with the direction of the missing momentum $\vec{q}(\vec{q} = \vec{p}_1 + \vec{p}_2 - \vec{p}_3 - \vec{p}_4)$. For such cases the directionvector of q has to be in the plane defined by the direction vectors of the two charged particles, whereas the sum of the angles between q and each of the two charged particles must be smaller than 180^o. As an example fig. 9 shows the distribution of $\cos\theta_{qn}$, where θ_{qn} is the angle between $\vec{q}$ and $\vec{n}$, the normal onto the directions of the two decay particles. Two-particle decays stand out as a spike at $\cos\theta_{qn} = 0$ in a selection in which the sum of the angles between q and each of the charged particles θ_{q+-} ($\theta_{q+-} = \theta_{q+} + \theta_{q-}$) is between 108^o and 198^o. It shows a smooth distribution (dashed line) with a wide

maximum for the kinematically impossible solution where $\theta_{q+-} = 198^o - 288^o$. From the figure it is clear that a fair amount of more body decays is present under the two-body decay peak. Full kinematic reconstruction assuming two-pion decay is being attempted at present, to reduce this background and improve the mass resolution. Because of the experimental uncertainties in momentum and direction measurements we select as candidates for two particle decays events with $\theta_{q+-} < 198^o$ and $| \cos\theta_{qn} | < 0.1$. Histograms with candidates for two-body and more-body decays, for both energies combined, are shown in fig. 10. Enhancements stand out in the 2-body decay spectra near the ρ and f masses and in the more body decay spectra near the ω and A_2 mass. We therefore tentatively identify the peaks with these resonances. The relative yields of these resonances can then be obtained by assuming a non-resonant background under the peaks, as indicated in fig. 10, and by taking the known branching ratios from two-and more-body decays into account. It is clear that this procedure is tentative at present as the background follows from eyeball fits and the number of peaks that can be resolved is determined by the mass resolution. The ratios of the yields thus found are given in table II, together with similar values in the same rapidity region obtained in a bubble chamber experiment at 12 and 24 GeV/c by the Bonn-Hamburg-München collaboration[4]. This group finds clear evidence for ρ and f excitation in $pp \rightarrow pp\pi^+\pi^-$ and of ω excitation in $pp \rightarrow pp\pi^+\pi^-\pi^o$.

As the present data are taken in a restricted region of momentum transfers t_1 and t_2, a further comparison with the lower energy data can only be made by assuming that the t-dependences for the production of the resonances is equal.

TABLE II

Ratios of cross-sections for production of mesonic resonances in $pp \to ppX$ for $|y_m| < 0.8$.

$\sqrt{s}$(GeV)	(ω/ρ)	$(\omega+\rho)/f$	A_2/f	$<-t_1>$ (GeV^2)	$<-t_2>$ (GeV^2)	
4.9	0.78 ± 0.13	3.3 ± 1.0	-			BHM-coll.
6.9	0.66 ± 0.13	0.89 ± 0.15	-			BHM-coll.
23.5	0.5 ± 0.25	1.1 ± 0.3	0.7 ± 0.2	0.22 ± 0.05		this exp.
30.5	0.8 ± 0.5	0.7 ± 0.3	0.8 ± 0.3	0.30 ± 0.07		this exp.

If the excitation of mesonic resonances is governed by Regge pole exchanges via the diagram indicated in fig. 1, one expects PP and Pf exchange to contribute to f-excitation and Pρ, Pω and PA_2 exchange to ρ, ω and A_2 excitation at high energies. The s-dependence of the ratio $(\rho+\omega)/f$ is consequently expected to be of the form

$$\frac{\sigma(pp \to pp\ (\rho+\omega))}{\sigma(pp \to pp\ f)} \propto s^{\alpha^{\rho,\omega} - \alpha^{P,f}} = s^{-\beta} \qquad (6)$$

If one takes $\alpha^\rho = \alpha^\omega = \alpha^f = 0.5$ and $\alpha^P = 1$, β will be of the order of 0 to 0.5. The experimental number derived from table II for $\sqrt{s} = 6.9$ GeV and above, $\beta = -0.02 \pm 0.10$, is in agreement with these expectations. The ratio increases at lower energies, presumably because other exchanges contribute[4]. The ratio (ω/ρ) seems to be s-independent. The s-dependence in the present data is compatible with $\beta = 0$, i.e. the absence of double Pomeron exchange. On the contrary, substantial contributions from odd G-and C-parity exchanges seem to be present.

References

1. M.G. Albrow et al., Phys. Letters 42B (1972) 279.

2. M.G. Albrow et al., Nucl. Phys. B102 (1976) 275.

3. M.G. Albrow et al., Inelastic scattering at the CERN ISR, to be published in Nuclear Physics B.

4. V. Blobel et al., Investigation of the reaction pp → pp + Meson Resonance at 12 and 24 GeV/c, Nucl. Phys. B69 (1974) 237.

Figure captions

Fig. 1 Diagram of low mass cluster production, with the exchange of Reggeons with trajectories α_1 and α_2 across rapidity gaps y_1 and y_2.

Fig. 2 Lines of equal mass and rapidity in x_1 vs x_2 plot at $\sqrt{s}$ = 23.5 GeV. Distortion of the straight lines of fixed rapidity by the effect of finite resolution is approximately taken into account by the hyperbola indicated. The FWHM resolution at this energy is indicated by the hatched area.

Fig. 3a) Missing mass resolution vs missing mass for events with $| y_m | < 0.8$.

b) Missing mass resolution vs rapidity of the central cluster at $\sqrt{s}$ = 23.5 to 61.6 GeV, computed from table I and equ. 3.

Fig. 4 x_1, x_2 scatter plot at $\sqrt{s}$ = 23.5 GeV for events with zero charged decay products of the central cluster. The mean momentum transfers are $\langle t_1' \rangle = -0.22$ GeV^2, $\langle t_2' \rangle = -0.05$ GeV^2. As $\langle -t_2' \rangle < \langle -t_1' \rangle$, the diffractive band near $x_2 = 1$ is more densily populated than the band near $x_1 = 1$.

Fig. 5 Missing mass spectra in pp → ppX at two energies. The mean momentum transfers of the two detected protons are indicated.

Fig. 6 Missing mass spectra in pp → ppX at two energies. Selection in which the directions of the charged decay products of X are limited between 28° and 152° in the c.m., i.e. pseudorapidity $|\eta_c| \lesssim 1.6$.

Fig. 7 Missing mass spectra in pp → ppX at s = 550 and 935 GeV^2 combined. Selection in which the decay products of X have zero charge.

Fig. 8 Missing mass spectra in $pp \to ppX$ at two energies. Selection in which only two charged decay particles of X are emitted and their directions are limited between 28° and 152° in the c.m., i.e. pseudo rapidity $|\eta_c| \lesssim 1.6$.

Fig. 9 Selection on angular criteria of 2-particle and more particle decay modes with $n_{ch} = 2$.

Fig. 10 Missing mass spectra at $s = 550$ and $935\ GeV^2$ combined; with two charged particles between 28° and 152°.
a) more-body decays of X
b) candidates for 2-body decays of X.
Lines for background subtraction under the resonances are indicated.

Fig. 11 Ratio of $(\rho+\omega)/f$ production in $pp \to pp$ + meson resonances.

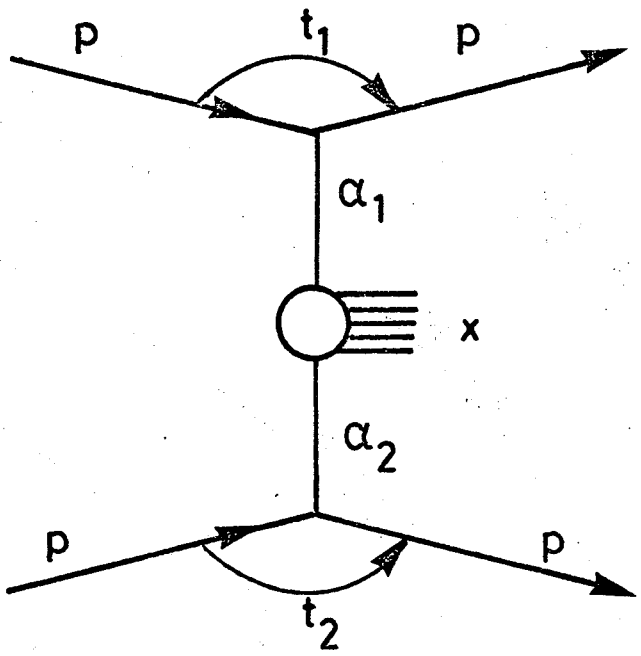

Fig.1

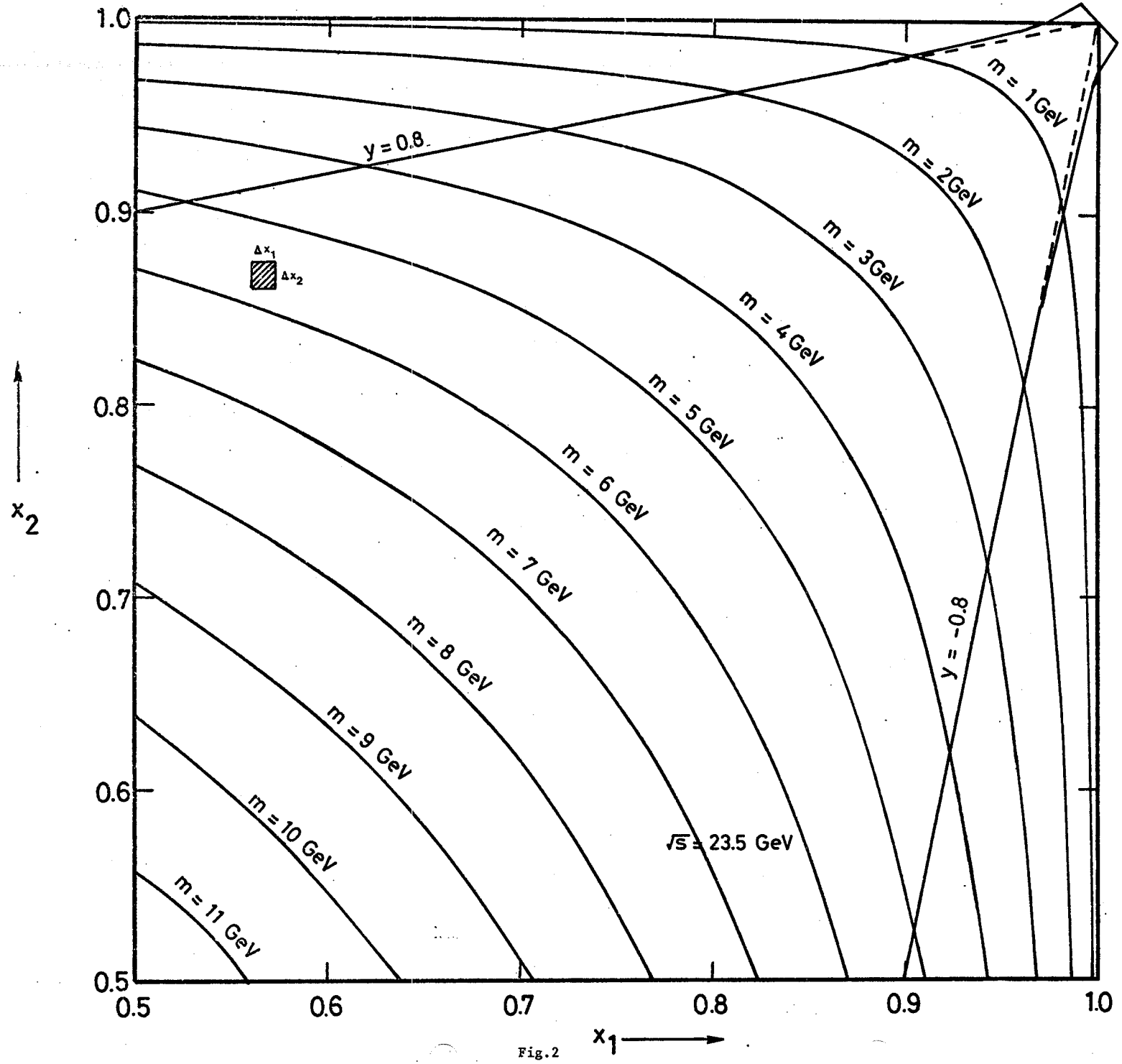
1.0
0.9
0.8
0.7
0.6
0.5
0.5
0.6
0.7
0.8
0.9
1.0
x_2
x_1
Δx_1
Δx_2
y = 0.8
y = -0.8
m = 1 GeV
m = 2 GeV
m = 3 GeV
m = 4 GeV
m = 5 GeV
m = 6 GeV
m = 7 GeV
m = 8 GeV
m = 9 GeV
m = 10 GeV
m = 11 GeV
$\sqrt{s}$ = 23.5 GeV

Fig.2

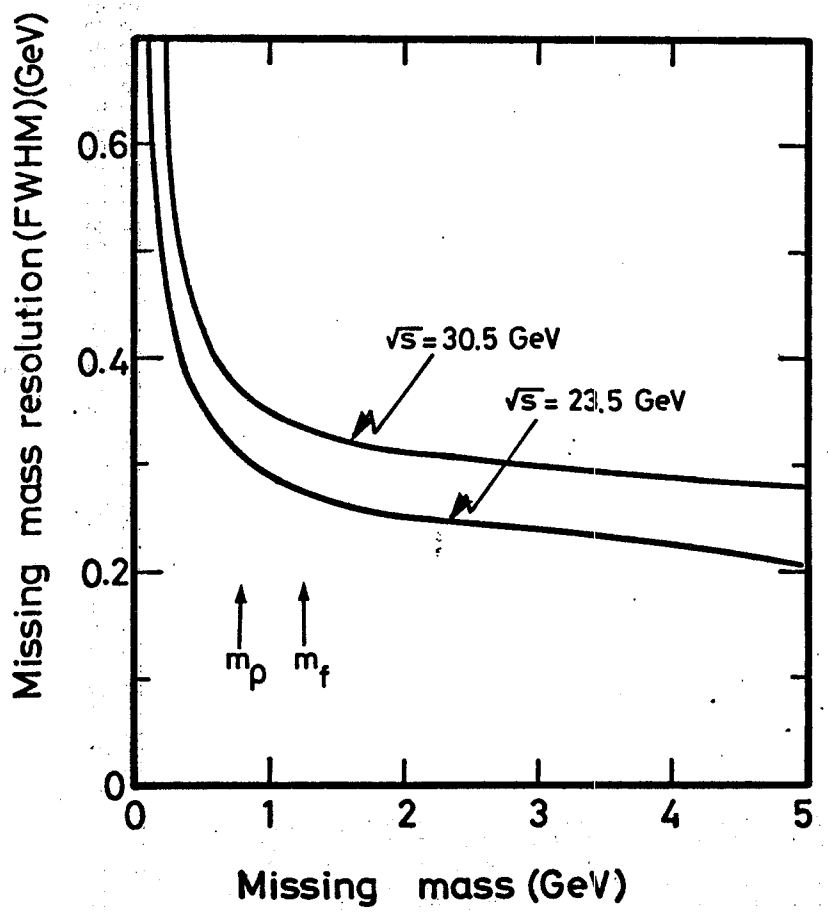
Missing mass resolution (FWHM)(GeV)
0.6
0.4
0.2
0
√s = 30.5 GeV
√s = 23.5 GeV
m_ρ
m_f
0
1
2
3
4
5
Missing mass (GeV)

Fig.3a

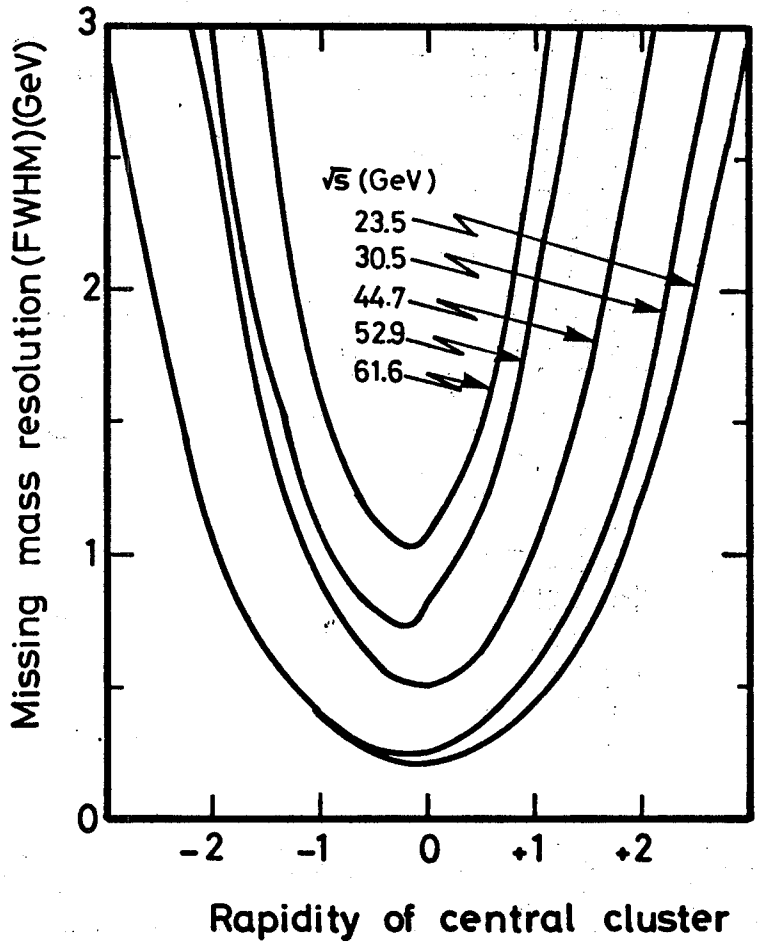
Missing mass resolution (FWHM)(GeV)
3
2
1
0
√s (GeV)
23.5
30.5
44.7
52.9
61.6
-2
-1
0
+1
+2
Rapidity of central cluster

Fig.3b

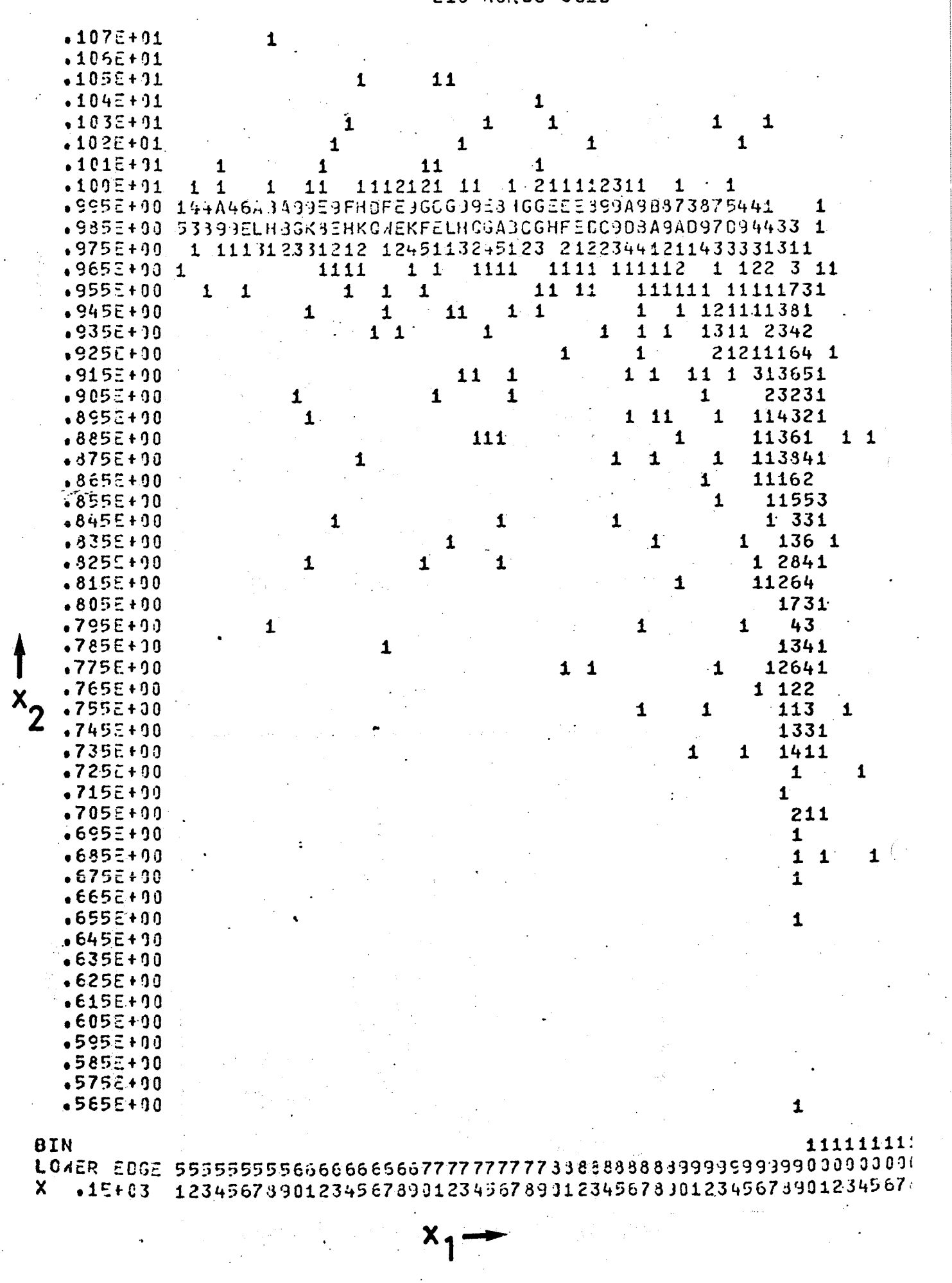
2-DIMENSIONAL HISTOGRAM NO. 30 X1 X2 M=0
218 WORDS USED
.107E+01
.106E+01
.105E+01
.104E+01
.103E+01
.102E+01
.101E+01
.100E+01
.995E+00
.985E+00
.975E+00
.965E+00
.955E+00
.945E+00
.935E+00
.925E+00
.915E+00
.905E+00
.895E+00
.885E+00
.875E+00
.865E+00
.855E+00
.845E+00
.835E+00
.825E+00
.815E+00
.805E+00
.795E+00
.785E+00
.775E+00
.765E+00
.755E+00
.745E+00
.735E+00
.725E+00
.715E+00
.705E+00
.695E+00
.685E+00
.675E+00
.665E+00
.655E+00
.645E+00
.635E+00
.625E+00
.615E+00
.605E+00
.595E+00
.585E+00
.575E+00
.565E+00
BIN
LOWER EDGE
X .1E+03
X2
X1

Fig.4

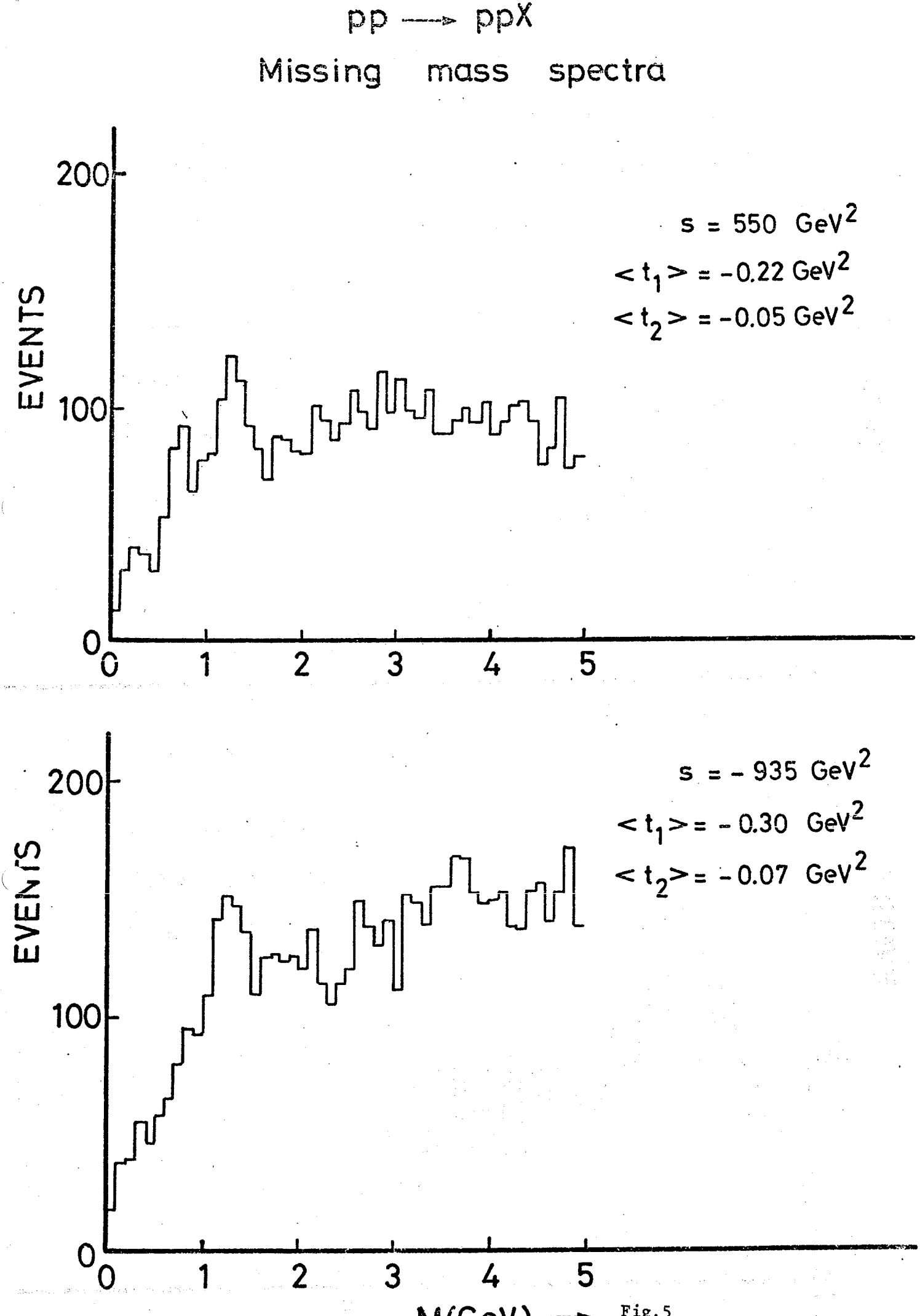
pp ⟶ ppX
Missing mass spectra
EVENTS
200
100
0
0
1
2
3
4
5
s = 550 GeV²
< t₁ > = -0.22 GeV²
< t₂ > = -0.05 GeV²
EVENTS
200
100
0
0
1
2
3
4
5
s = - 935 GeV²
< t₁ > = - 0.30 GeV²
< t₂ > = - 0.07 GeV²
M(GeV) ⟶

Fig.5

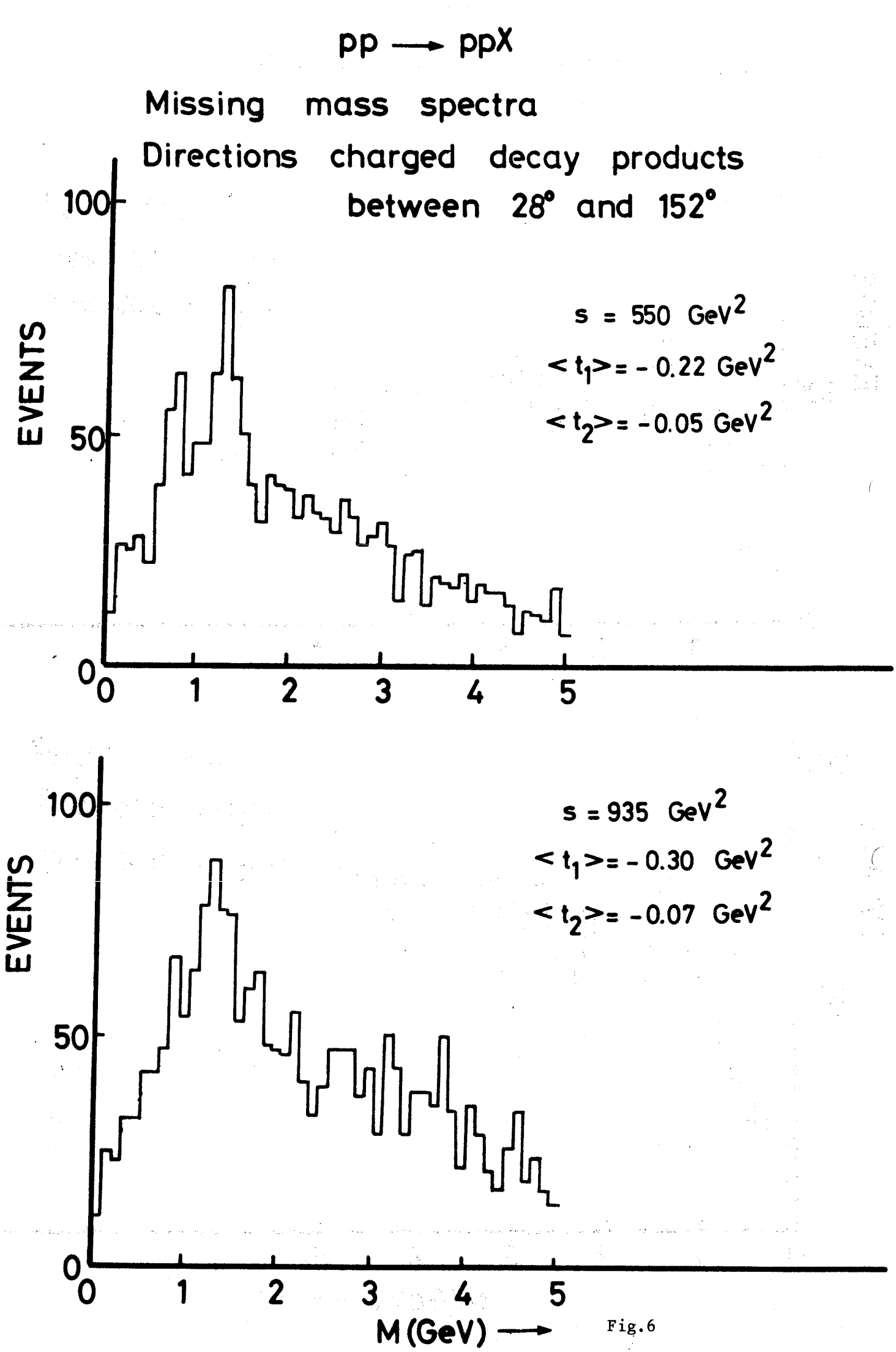
pp ⟶ ppX
Missing mass spectra
Directions charged decay products
between 28° and 152°
EVENTS
100
50
0
0
1
2
3
4
5
s = 550 GeV²
< t₁ > = - 0.22 GeV²
< t₂ > = - 0.05 GeV²
EVENTS
100
50
0
0
1
2
3
4
5
M (GeV) ⟶
s = 935 GeV²
< t₁ > = - 0.30 GeV²
< t₂ > = - 0.07 GeV²

Fig.6

$pp \longrightarrow ppX$

Missing mass spectrum $s = 550$ and $935\ GeV^2$

Zero charge decay products

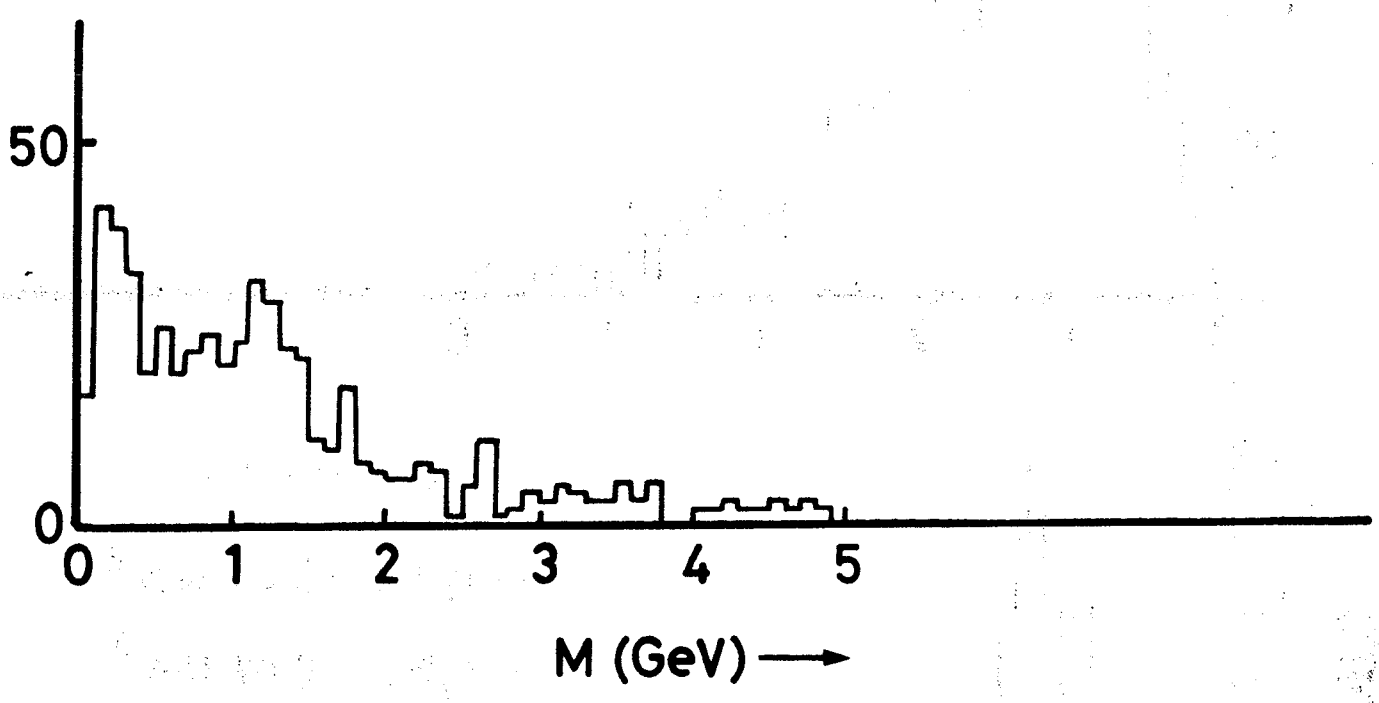

Fig.7

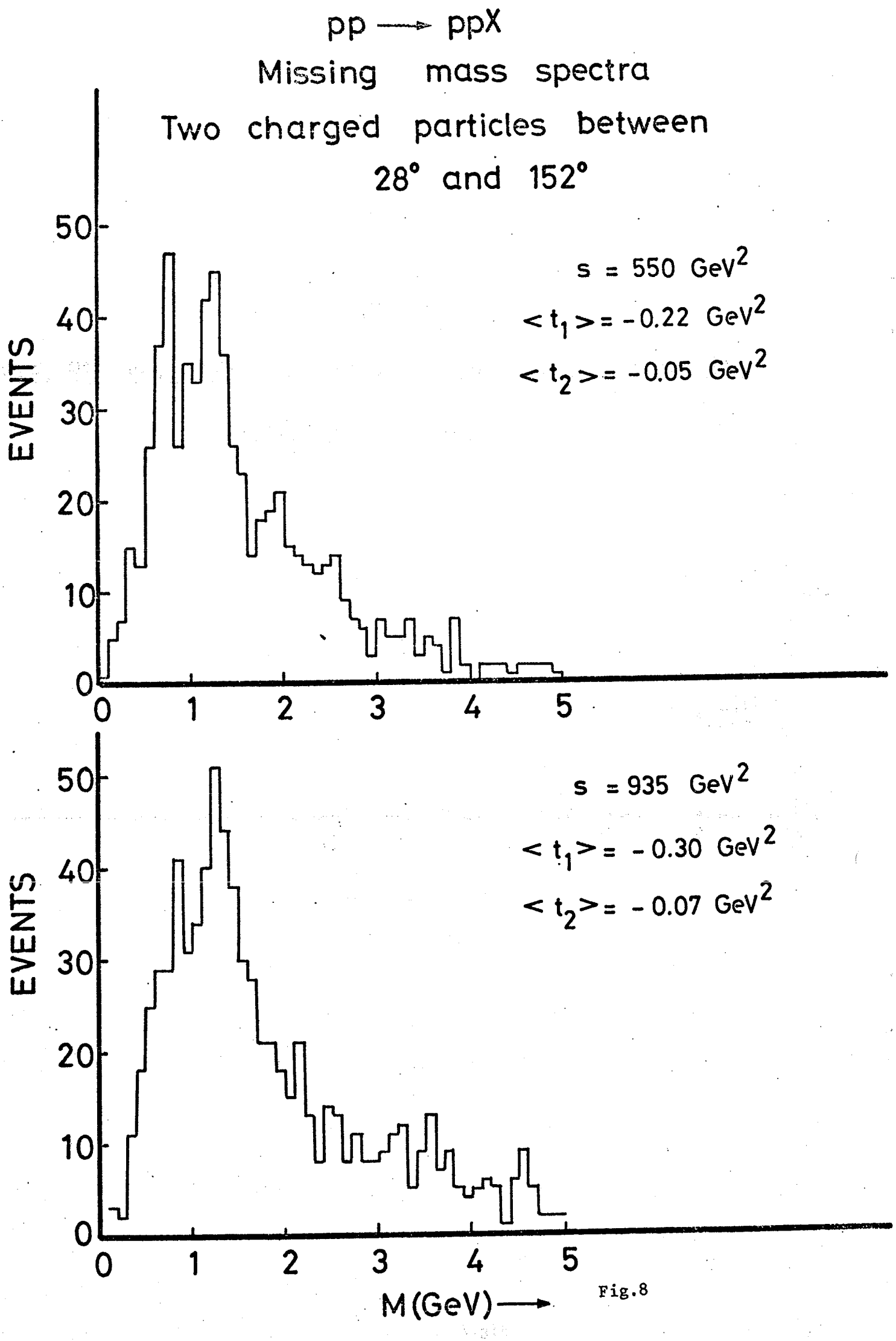
pp ⟶ ppX
Missing mass spectra
Two charged particles between
28° and 152°
s = 550 GeV²
< t₁ > = -0.22 GeV²
< t₂ > = -0.05 GeV²
EVENTS
0
10
20
30
40
50
0
1
2
3
4
5
s = 935 GeV²
< t₁ > = -0.30 GeV²
< t₂ > = -0.07 GeV²
EVENTS
M(GeV) ⟶

Fig.8

Selection of 2-particle decay modes in $pp \longrightarrow pp + 2$ charged particles

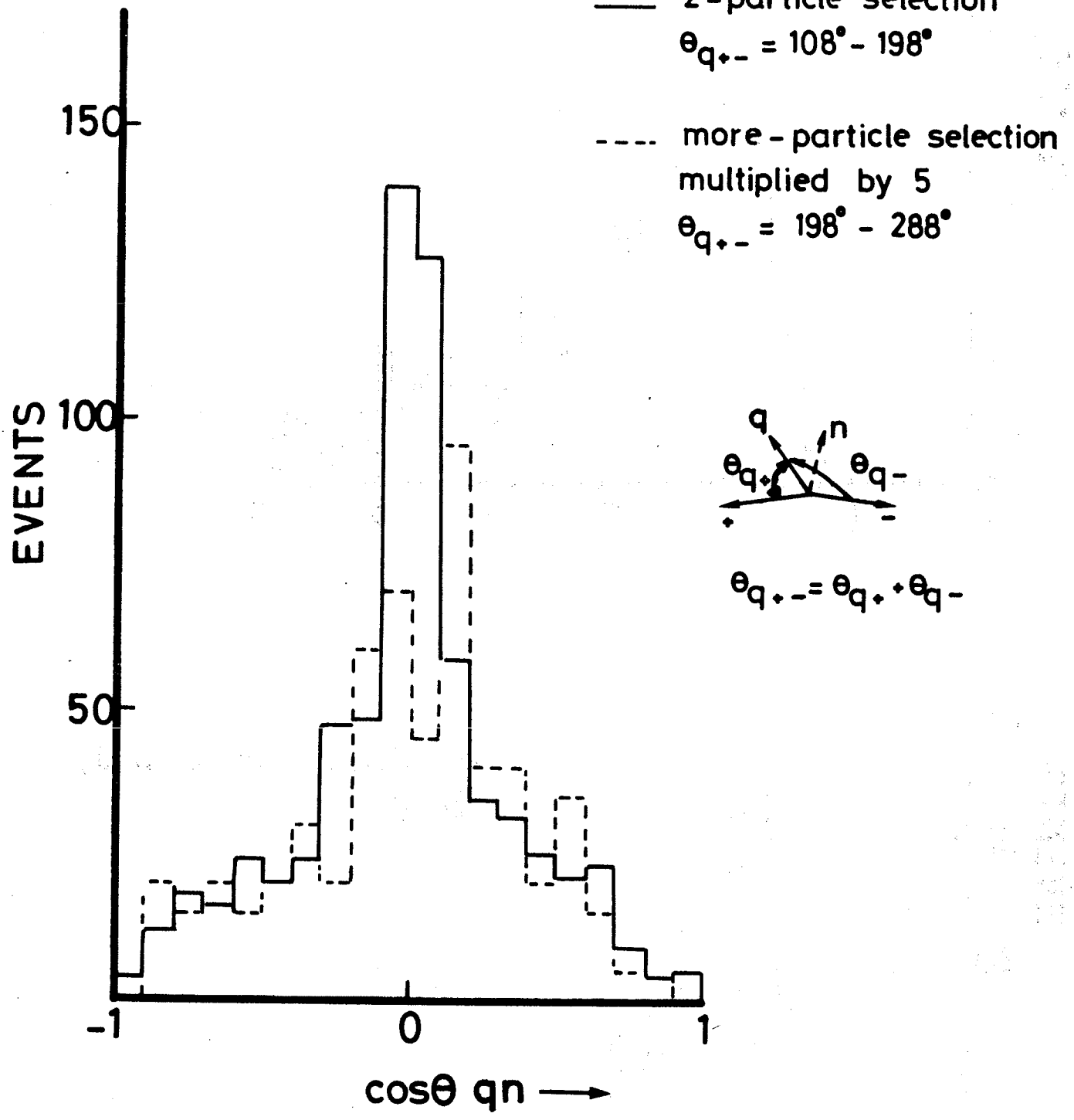

Fig.9

$pp \longrightarrow ppX$

Missing mass spectra at $s = 550$ and 935 GeV^2
two charged particles between 28° and 152°

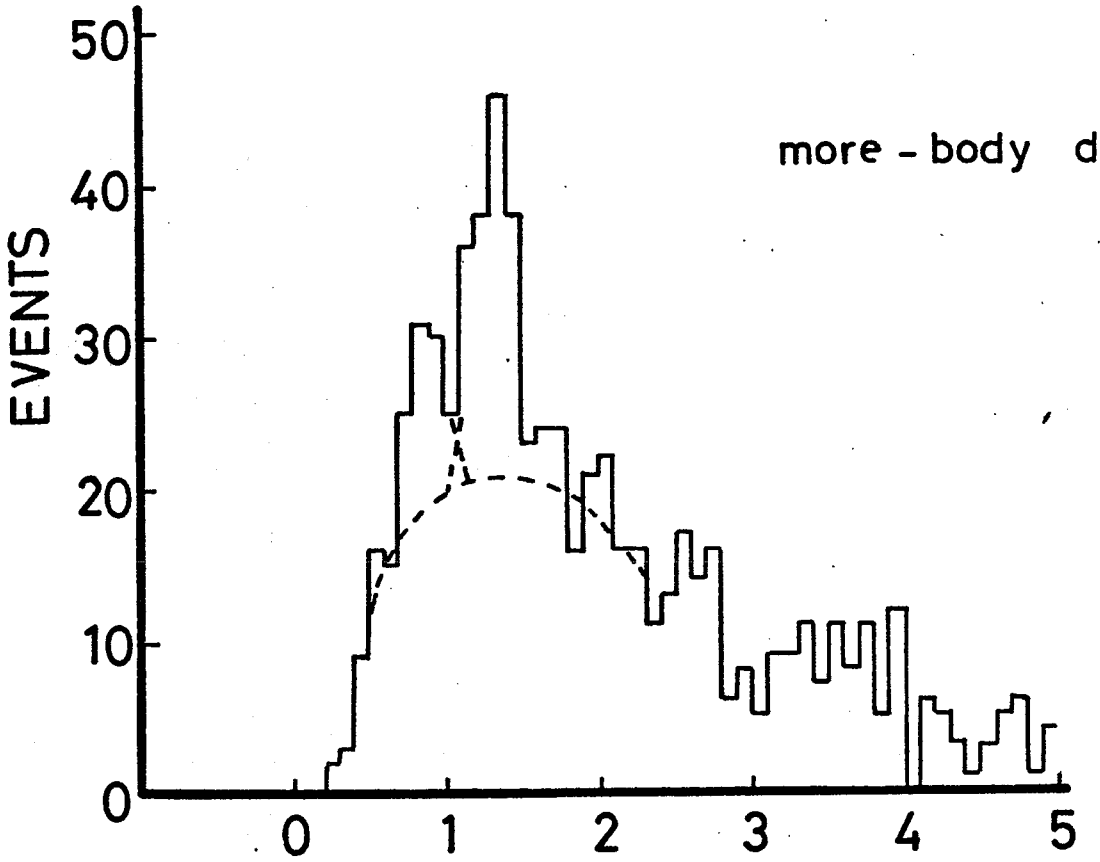

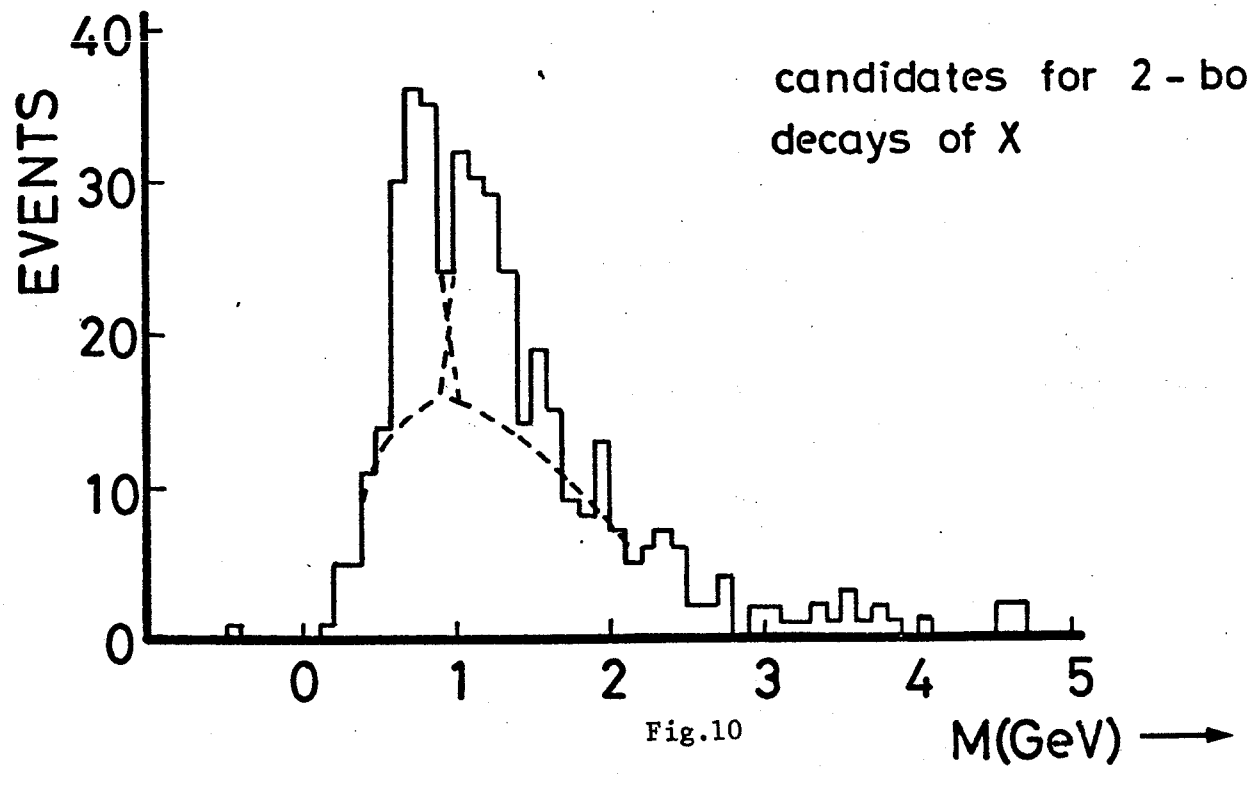

Fig.10

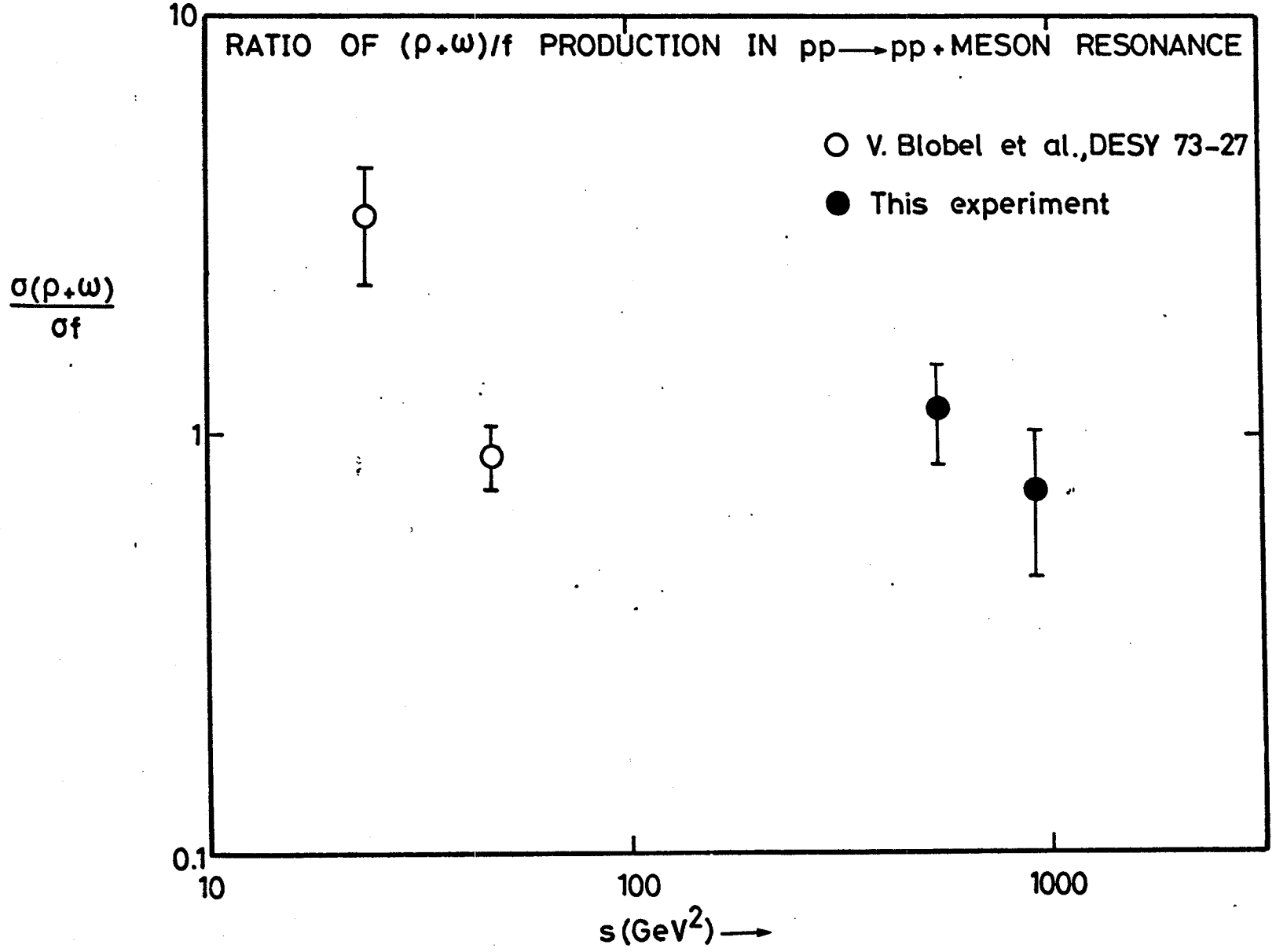
RATIO OF (ρ+ω)/f PRODUCTION IN pp⟶pp+MESON RESONANCE
O V. Blobel et al.,DESY 73-27
● This experiment
σ(ρ+ω)/σf
10
1
0.1
10
100
1000
s (GeV²) ⟶

Fig.11